

JGR Space Physics

RESEARCH ARTICLE

10.1029/2020JA028525

Key Points:

- Case study for beam-driven whistler mode waves associated with magnetic reconnection near the dayside magnetopause
- Quantitatively testing the Landau resonance condition and solving kinetic dispersion relations suggest whistler generation by electron beams
- Whistlers provide efficient electron pitch-angle scattering in the high-energy range (300–3,000 eV), which can isotropize electrons and exchange energy between plasmas and waves

Correspondence to:

C. J. Xiao,
cjxiao@pku.edu.cn

Citation:

Zhao, S. Q., Xiao, C. J., Liu, T. Z., Chen, H., Zhang, H., Shi, M. J., et al. (2021). Observations of the beam-driven whistler mode waves in the magnetic reconnection region at the dayside magnetopause. *Journal of Geophysical Research: Space Physics*, 126. <https://doi.org/10.1029/2020JA028525>

Received 11 AUG 2020

Accepted 25 DEC 2020

Observations of the Beam-Driven Whistler Mode Waves in the Magnetic Reconnection Region at the Dayside Magnetopause

S. Q. Zhao^{1,2}, C. J. Xiao¹, Terry Z. Liu^{3,8}, Huayue Chen⁴, H. Zhang³, M. J. Shi⁵, Shangchun Teng⁴, H. S. Zhang², X. G. Wang⁶, Z. Y. Pu⁷, and M. Z. Liu⁹

¹Fusion Simulation Center, State Key Laboratory of Nuclear Physics and Technology, School of Physics, Peking University, Beijing, China, ²Deutsches Elektronen Synchrotron (DESY), Zeuthen, Germany, ³Geophysical Institute, University of Alaska, Fairbanks, AK, USA, ⁴CAS Key Laboratory of Geoscience Environment, School of Earth and Space Sciences, University of Science and Technology of China, Hefei, China, ⁵Shandong Key Laboratory of Optical Astronomy and Solar-Terrestrial Environment, Institute of Space Sciences, Shandong University, Weihai, China,

⁶Department of Physics, Laboratory for Space Environment and Physical Sciences, Harbin Institute of Technology, Harbin, China, ⁷School of Earth and Space Sciences, Peking University, Beijing, China, ⁸Cooperative Programs for the Advancement of Earth System Science, University Corporation for Atmospheric Research, Boulder, CO, USA, ⁹LESIA, Observatoire de Paris, Université PSL, CNRS, Sorbonne Université, Université de Paris, Meudon, France

Abstract We report observations of the whistler mode waves in the magnetic reconnection region at the dayside magnetopause using the magnetospheric multiscale (MMS) mission on January 11, 2016. In this event, whistlers mostly occur on the magnetospheric side of the reconnection central plane and are closely related to counter-streaming electron beams in the medium energy range (200–300 eV). These counter-streaming electron beams can be attributed to the accelerated magnetosheath electrons by the reconnection. Through quantitatively testing the Landau resonance condition and solving the kinetic dispersion relations, we present the evidence for whistler excitation by electron beams in the medium energy range. Additionally, the whistlers are observed simultaneously with the pitch-angle scattering of electrons in the high-energy range (300–3,000 eV). The calculation results show that this scattering is likely to occur through electron cyclotron wave-particle interactions, which can isotropize electrons and exchange energy between plasmas and waves.

1. Introduction

Magnetic reconnection is a fundamental energy conversion process that transfers magnetic energy into plasma kinetic and thermal energy via reconfiguration of magnetic topology (e.g., Dungey, 1961; Xiao et al., 2007). Magnetic reconnection plays a crucial role in space weather-related phenomena. For example, at the Earth's magnetopause, magnetic reconnection is regarded as the main gateway wherein solar wind plasmas transfer material, momentum, and energy to the magnetosphere (Fuselier et al., 2011). Reconnection is also associated with a variety of wave modes, including the high-frequency electrostatic waves (e.g., Zhou et al., 2016), the medium-frequency whistler mode waves (e.g., Cao et al., 2017), the lower hybrid waves (e.g., Vörös et al. 2019), the low-frequency kinetic Alfvén waves (e.g., H. Huang et al. 2018), and the Alfvén-whistler waves (Wang et al., 2000). These waves could accelerate and heat plasmas. Therefore, it is crucial to investigate the excitation mechanisms of these waves and their effects on magnetic reconnection.

This study focuses on the frequently observed whistler mode waves and explores their association with reconnection. Whistlers are electromagnetic waves in the frequency range between the lower hybrid frequency (f_{LH}) and the electron cyclotron frequency (f_{ce}). Whistlers are typically characterized by high polarization, high ellipticity (right-handed circularly polarized waves), and high-electromagnetic planarity. Previous studies have reported that whistler mode waves can modulate the reconnection process (Deng & Matsumoto, 2001) and cause electron acceleration in reconnection (Drake et al., 2008). Whistlers can also efficiently scatter pitch angles of the electrons, which relaxes temperature anisotropies in electron velocity distributions (Khotyaintsev et al., 2011) and randomizes wave energy to plasma energy.

Two most common excitation mechanisms of whistler mode waves are the cyclotron resonance with anisotropic electrons ($\omega - k_{\parallel}v_{\parallel} = \omega_{ce}$) and the Landau resonance with electron beams moving along the magnetic

field ($\frac{\omega}{k_{\parallel}} = v_{\parallel}$), where k_{\parallel} is the parallel wave number, v_{\parallel} is the parallel component for a given resonance velocity of electrons, and ω_{ce} is the electron cyclotron frequency (Kennel & Petschek, 1966; Wilder et al., 2017). Whistlers can also be triggered by heat flux instabilities (Gary et al., 1994) and Čerenkov emission (Goldman et al., 2014). In the context of reconnection, different types of velocity distributions can lead to different excitation mechanisms. Wilder et al. (2017) suggested that whistler mode waves have both anisotropy and beam-driven components by qualitatively analyzing the reduced distributions. However, the beam-driven whistler mode waves remain to be studied quantitatively.

In this study, using the magnetospheric multiscale (MMS) measurements, we report observations of the whistler mode waves in the magnetic reconnection region at the dayside magnetopause and present quantitative analysis results for their excitation mechanisms. The outline of this paper is as follows. After a brief introduction in Section 1, data sets and analysis methods are shown in Section 2. In Section 3, we notice that the whistlers are closely related to counter-streaming electron beams in the medium energy range (200–300 eV) and electron pitch-angle scattering in the high energy range (300–3,000 eV) through comparing observations on both sides of the central plane. Moreover, we discuss a potential excitation mechanism of whistlers by quantitatively testing the Landau resonance condition and solving the kinetic dispersion relations. In Section 4, we discuss and conclude our results.

2. Methodology

2.1. Data

We use data from the MMS mission, consisting of four identically instrumented spacecraft (Burch et al., 2016). In this study, magnetic field data are from the fluxgate magnetometer (FGM, 128 samples/s in burst mode and 16 samples/s in survey mode) (Russell et al., 2016) and the search-coil magnetometer (SCM; 8,192 samples/s; Contel et al., 2016). The electric field data with the sampling rate of 8,192 Hz are from the spin-plane double probes (SDP; Lindqvist et al., 2016) and the axial double probes (ADP; Ergun et al., 2016). The plasma data are from the fast plasma investigation (FPI; Pollock et al., 2016) with a superb temporal resolution of 30 ms for electrons and 150 ms for ions. We use interplanetary magnetic fields and plasma data from the *Wind* mission (Lepping et al., 1995; Lin et al., 1995).

2.2. Methods for Obtaining Dispersion Relations

We utilize the Singular Value Decomposition (SVD) method (Santolík et al., 2003) by solving the linearized Faraday's law: $\mathbf{k} \times \mathbf{E} = \omega \mathbf{B}$ to determine the observed wave vectors. The complex amplitude matrices of electric and magnetic fields (\mathbf{E} and \mathbf{B}) are from the cross wavelet transform based on the Morlet wavelet analysis (Grinsted et al., 2004). In this way, we can obtain the observed dispersion relations and the associated phase speeds, which are crucially essential for quantitatively analyzing wave excitation mechanisms.

Moreover, we utilize the BO ("wave" in Chinese) method (Xie, 2019) for plasma waves and instability analysis. Using this numerical method, we can calculate the kinetic dispersion relations with an arbitrary number of species and an extended Maxwellian based equilibrium distribution. We use the electron distribution in the $V_B - V_V$ plane at a 30 ms interval, where V_B is parallel to the magnetic field and V_V is in the $(\mathbf{v} \times \mathbf{b}) \times \mathbf{b}$ direction (\mathbf{b} and \mathbf{v} are the unit vectors of the magnetic field and the electron bulk velocity). The two dimensional cut is integrated over all available velocities in the third direction. As shown in Figure 7a later, electrons mainly move parallel and antiparallel to the magnetic field. Therefore, we try to simplify the electron distribution and model the distribution function as a sum of bi-Maxwellian distributions, including parallel and antiparallel beams.

$$f(v_{\parallel}, v_{\perp}) = \sum_i \frac{n_i}{\pi^{3/2} v_{T\perp}^2 v_{T\parallel}} \exp\left(-\frac{v_{\perp}^2}{v_{T\perp}^2} - \frac{(v_{\parallel} - v_b)^2}{v_{T\parallel}^2}\right) \quad (1)$$

where i represents different particle populations, n_i is the density, v_b is the beam velocity, and v_{\parallel} and v_{\perp} are the electron velocities parallel and perpendicular to magnetic fields. $v_{T\parallel}$ and $v_{T\perp}$ are parallel and perpendicular thermal velocities, and corresponding temperatures are $T_{\parallel} = \frac{1}{2}m_e v_{T\parallel}^2$ and $T_{\perp} = \frac{1}{2}m_e v_{T\perp}^2$. The fitting parameters are treated as input into the BO method to calculate waves' theoretical dispersion relations and the associated growth rate.

3. Observations of the Whistler Mode Waves in the Dayside Reconnection Region

3.1. Overview

Figure 1 shows MMS2 observations in the dayside reconnection region on January 11 2016. Data are shown in local magnetic normal (LMN) coordinates obtained from the Minimum Variance Analysis of magnetic fields (B. Sonnerup & Scheible, 1998) during 06:52:46–06:52:50 Universal Time (UT). The eigenvectors are $L = [0.23, 0.36, 0.91]$, $M = [0.03, -0.93, 0.36]$, and $N = [0.97, -0.05, -0.23]$ in geocentric solar ecliptic (GSE) coordinates, respectively, where L is along the reconnecting field, M is in the guide field direction, and N is along the magnetopause normal. At 06:53:00 UT, the MMS2 was located at $[9.8, -4.4, -1.0]_{GSE}$ Earth radii (R_E). The solar wind speed was ~ 390 km/s from the Wind spacecraft at $[236.1, -32.8, 16.0]_{GSE} R_E$. Therefore, the interplanetary magnetic field (IMF) should be shifted by ~ 62 min to match MMS2 measurements. At around 05:50:00 UT, Wind spacecraft observed $[3, -8, -2]_{GSE}$ nT, southward IMF.

Figure 1b shows that magnetic fields observed by MMS change from northward ($B_L > 0$) to southward ($B_L < 0$), indicating an outbound magnetopause crossing from the magnetosphere to the magnetosheath at $\sim 06:52:48.16$ UT (Figure 1②). Meanwhile, Figures 1c and 1d show that high-speed ion and electron jets along the L direction (V_{iL} and V_{eL}) rotate from southward to northward, suggesting the spacecraft traveling from the south to the north of the magnetic X-line. The MMS2 trajectory is shown in Figure 2. Figure 1c shows that the V_{iL} reaches up to ~ 390 km/s on the magnetospheric side of the current sheet and ~ 165 km/s on the magnetosheath side. Figures 1k and 1l display the Walén relations on the magnetospheric side (06:52:30.0–06:52:48.5 UT) and on the magnetosheath side (06:52:48.5–06:53:15.0 UT), respectively. We can see that the ion bulk velocities in the De_Hoffmann-Teller frame are highly correlated with the local Alfvén velocities (the absolute values of slopes approach to 1, and linear correlation coefficients are ~ 0.99 and 0.98, respectively), indicating the appearance of a reconnecting ion outflow on each side (B. U. Ö. Sonnerup et al., 1987).

It is not a strictly symmetric reconnection because though the magnetic field magnitude ($|B|$) is steady at ~ 45 nT (Figure 1a), the density ratio is $\sim 1:4$ (Figure 1e) during this crossing. The out-of-plane guide magnetic field (B_M) is as large as the asymptotic magnetic field ($B_{L,0}$). Figure 1f shows a significant enhancement of the current from $\sim 06:52:30$ UT, indicating that MMS2 enters the current sheet at this moment. Moreover, the electric fields, accompanied by the reversals of ion and electron bulk flows, are principally balanced by plasma convection (Figure 1g). In Figure 1h, ion perpendicular temperature is higher than the parallel temperature, and ion temperature anisotropy increases significantly across the current sheet. However, for electrons, the perpendicular temperature is lower than the parallel temperature. Moreover, the electron temperature near the X-line is much higher than that in the exhaust region. Figures 1i and j show the spectrogram of ion (electron) differential energy fluxes. The ion energy fluxes shift into lower energy levels with an intensity reduction, and the electron energy fluxes show significant enhancement across the current sheet.

3.2. Observations of the Whistler Mode Waves

Figure 3 shows MMS2 measurements on the magnetospheric side of the reconnection central plane during 06:52:34–06:52:40 UT. Magnetic field and plasma data are shown in LMN coordinates, the same as in

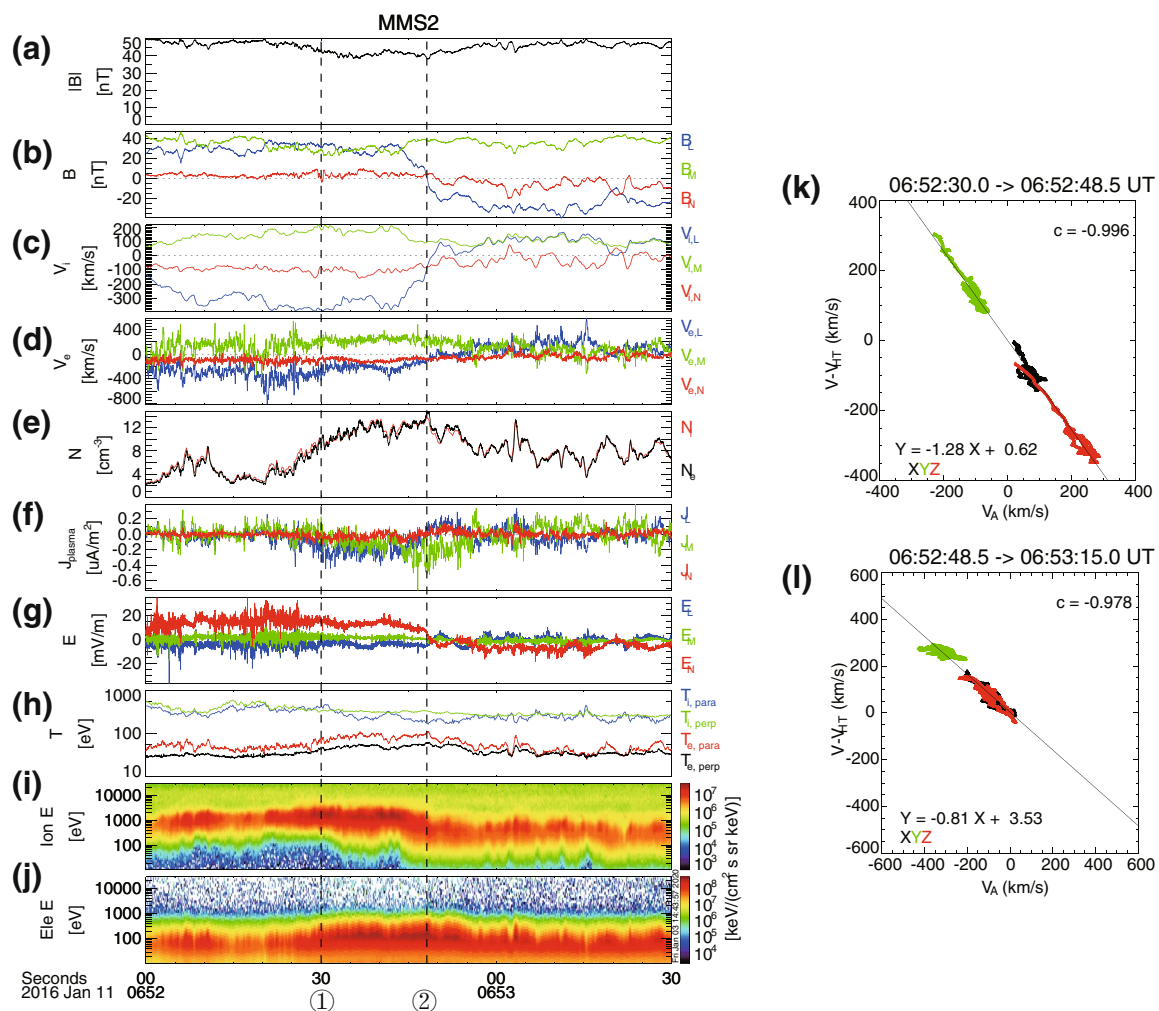


Figure 1. Overview of a reconnection region observed by MMS2 during 06:51:58–06:53:30 UT on January 11, 2016 in LMN coordinates. (a) Magnetic field magnitude $|B|$; (b) magnetic field components; (c) ion bulk velocity components; (d) electron bulk velocity components; (e) ion and electron density; (f) plasma current density; (g) electric field components; (h) ion and electron temperature; (i) ion and (j) electron spectrograms, respectively; (k) and (l) scatters showing correlations of local Alfvén velocity and the ion bulk velocity in the De_Hoffmann-Teller frame, where the parameter c is the linear correlation coefficient. $L = [0.23, 0.36, 0.91]$, $M = [0.03, -0.93, 0.36]$, and $N = [0.97, -0.05, -0.23]$ GSE. LMN, Local Magnetic Normal; GSE, Geocentric Solar Ecliptic; MMS, Magnetospheric Multiscale mission.

Figure 1. Electrons are observed with bi-directional pitch angle distributions both in the low (30–200 eV) and medium (200–300 eV) energy range, indicating that magnetic field lines are closed (Figures 3f and 3g). In the medium energy range, the presence of the counter-streaming electron beams is accompanied with significant enhancement of magnetic field wave power at $0.1f_{ce} - 0.5f_{ce}$ (Figures 3g and 3i). These counter-streaming electron beams can be attributed to accelerated magnetosheath electrons by the reconnection (Egedal et al., 2011). In the high-energy range, butterfly like pitch angle distributions with a minimum flux at $\sim 90^\circ$ are presented (Figure 3h). The period of the intense magnetic fluctuations corresponds to the period of electron pitch-angle scattering.

Figure 4 shows MMS2 measurements on the magnetosheath side of the reconnection central plane during 06:52:50–06:53:10 UT, in the same format as Figure 3. Unlike the observations on the magnetospheric side, magnetic fluctuations ($0.1f_{ce} - 0.5f_{ce}$) are rarely observed, except at $\sim 06:52:55$ UT (Figure 4i). In the medium energy range, electron energy fluxes show significant enhancement in the parallel and perpendicular direction (Figure 4g), rather than the counter-streaming beams (Figure 3g). The increase of electron energy fluxes at $\sim 90^\circ$ is comparable to that along the magnetic field. In the high-energy range, electron pitch-angle

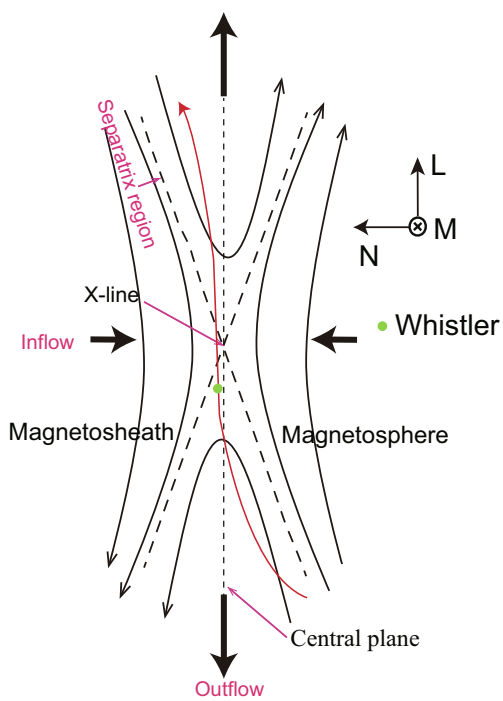


Figure 2. A schematic of the MMS2 trajectory across the reconnection region (red curve) and the location of whistlers at $\sim 06:52:48$ UT (green point) in LMN coordinates. LMN, Local Magnetic Normal; MMS, Magnetospheric Multiscale mission.

The frequency f corresponding to the maximum of magnetic PSD and the f_{ce} are marked by black and pink horizontal lines, respectively (Figures 6c–6i). Figure 6e illustrates that the ratio of electric over magnetic wavefield is much less than the speed of light at the frequency f , suggesting that the waves have much stronger magnetic power than electric power.

Figures 6f–6i shows the wave properties, including the ellipticity, wave propagation angle (θ), electromagnetic planarity (F_{EB}), and field-aligned Poynting flux. Figure 6f shows that the wave train at the frequency f exhibits ellipticity close to +1 and therefore is right-handed circularly polarized (e.g., Wilder et al., 2017). Additionally, Figure 6g shows that the θ is mostly larger than 160° , meaning that the waves propagate approximately antiparallel to the magnetic field. As F_{EB} is close to 1, the assumption of plane waves stands (Figure 6h). All these properties determined using the SVD method (Santolík et al., 2003) are consistent with the wave train being whistler mode waves.

3.3. Electron Distribution and Instability Analysis

A necessary condition for determining wave vectors by the SVD method is that the assumption of plane waves stands (Santolík et al., 2003). Since F_{EB} is relatively stable and close to 1 during 06:52:48.56–06:52:48.59 UT in Figure 6h; thus, we select this duration to conduct quantitative calculation and analysis. We shift wave frequencies from the spacecraft frame into the plasma flow frame. When magnetic PSD is close to the maximum ($f \sim 0.25 f_{ce}$), the 95% confidence interval of observed wave vectors $k_{\parallel} = (-0.43 \pm 0.014) / d_e$, where the electron cyclotron frequency $f_{ce} \sim 1100$ Hz and the electron skin depth $d_e \sim 1.4$ km. Consequently, the observed phase speed (V_{phase}) of the whistlers is $\sim -5,700$ km/s.

Figure 7a shows the electron velocity distribution in the $V_B - V_V$ plane during 06:52:48.571–06:52:48.601 UT. Clearly, four populations can be distinguished with different energy ranges and pitch angles: the parallel

distributions are similar to those in the medium energy range (Figure 4h), whereas butterfly like pitch angle distributions can be observed in the presence of waves on the magnetospheric side (Figure 3h). Therefore, we hypothesize that the waves are closely related to the counter-streaming electron beams in the medium energy range and the electron pitch-angle scattering in the high-energy range.

To analyze more explicit properties of the waves, we zoom in to a smaller timescale from 06:52:47 to 06:52:50 UT. Figures 5a–5c suggest that the intense magnetic fluctuations ($0.1 f_{ce} - 0.5 f_{ce}$) occur between the flow stagnation point and the in-plane magnetic null (green dot in Figure 2). We apply cross wavelet transform to magnetic and electric fields to get their spectral matrices of complex amplitudes. Then we take the matrices as input into the SVD method (Santolík et al., 2003) to determine wave vectors. Figures 5d and 5f illustrate spectrograms of wave vectors in field-aligned coordinate obtained using the FGM data in survey mode (16 samples/s). We can see that wave vectors are relatively stable, and the waves mainly propagate along the antiparallel magnetic field during 06:52:48.52–06:52:48.62 UT.

Figure 6 displays the PSD and other properties of the electromagnetic waves during 06:52:48.52–06:52:48.62 UT. The whistlers likely have harmonics in the electric fields. Figures 6a and 6b show electric field from electronic data processing (EDP) and magnetic fields from SCM in field-aligned coordinates (at 8,192 samples/s). Figures 6c and 6d show the electric and magnetic PSD in the range of 30–4,096 Hz. The electrostatic solitary waves exist at the f_{ce} , which can be seen from the parallel electric field (red line in Figure 6a) and the electric PSD (Figure 6c). Figure 6d shows the significant enhancement of magnetic PSD from 100 to 500 Hz.

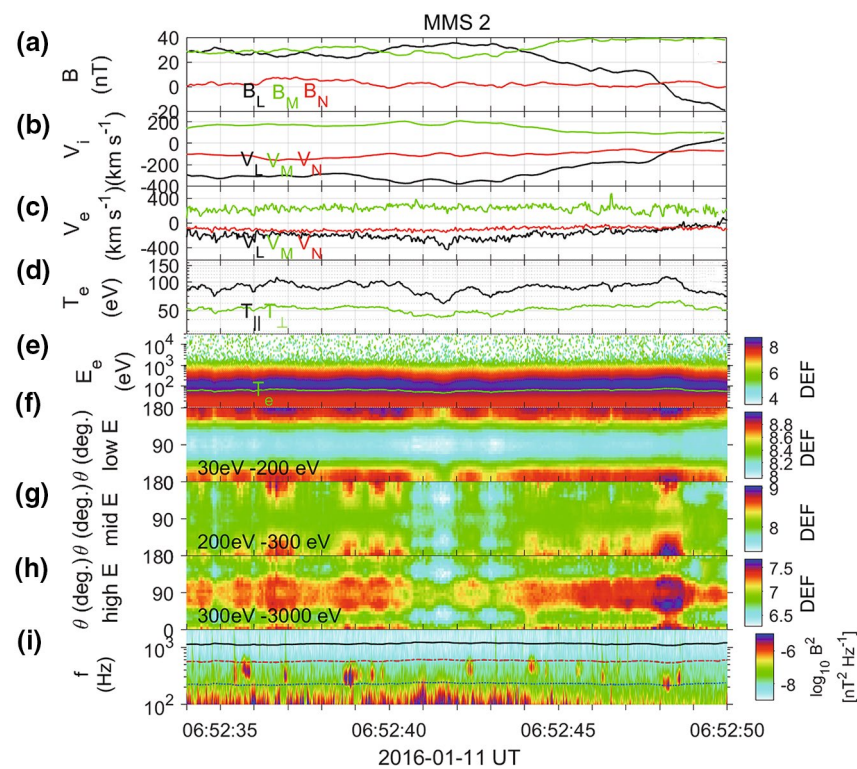


Figure 3. MMS2 measurements on reconnection central plane's magnetospheric side in LMN coordinates during 06:52:34–06:52:40 UT. (a) Magnetic field components; (b) ion bulk velocity components; (c) electron bulk velocity components; (d) electron temperature; (e) electron spectrogram of differential energy flux (DEF, the color scale is in units of $\text{eVs}^{-1}\text{cm}^{-2}\text{sr}^{-1}\text{eV}^{-1}$); (f–h) electron pitch-angle distributions for three energy ranges from low (30–200 eV), medium (200–300 eV), to high (300–3,000 eV) energy; (i) the power spectral distribution of the magnetic field. The horizontal lines represent the electron cyclotron frequency f_{ce} (black), $0.5f_{ce}$ (red), and $0.1f_{ce}$ (blue), respectively. LMN, Local Magnetic Normal; MMS, Magnetospheric Multiscale mission.

beam (pitch angle $\sim 0^\circ - 20^\circ$), the antiparallel beam (pitch angle $\sim 160^\circ - 180^\circ$), high-energy background electrons, and low-energy background electrons. To quantitatively calculate the plasma parameters such as electron density, electron temperature, and electron bulk velocity, we model the electron distribution function as a sum of bi-Maxwellian distributions, including parallel and antiparallel drift (Equation 1). Figure 7b shows the phase space density in the parallel (red) and perpendicular (black) directions. The dashed lines represent the observed distributions, and the solid lines represent the fitted distributions. The fitting parameters shown in Table 1 are treated as input into the BO method to evaluate whistlers' theoretical dispersion relations and growth rate.

The speeds of electron parallel beams (V_{para}) and antiparallel beams (V_{anti}) are $\sim 6,600 \text{ km/s}$ and $\sim -6,900 \text{ km/s}$, respectively. It is noteworthy that the electron beam speeds are close to and slightly larger than whistlers' phase speed ($V_{\text{phase}} \sim -5,700 \text{ km/s}$). Therefore, one possibility is that the whistler mode waves are driven by the electron beams. The electron beams resonate with the waves contributing to the inverse Landau damping process that converts plasma energy into wave energy.

To confirm this, we calculate whistlers' theoretical dispersion relations and the linear growth rate γ from the BO method (Xie, 2019). In this process, we set the wave propagation angle as 180° and input the fitting parameters in Table 1. Figure 7c shows that γ is positive at $0.27 < kd_e < 0.62$, indicating that waves can be excited in this environment. The growth rate γ reaches the maximum at $kd_e \sim 0.53$, consistent with the observed wave vectors ($k_{\parallel} = (-0.43 \pm 0.014)/d_e$). The small deviation of wave vectors may partly come from observational and computational errors. Besides, k is the wave vector, whereas observational k_{\parallel} is the parallel component of the wave vector. We notice that the wave frequency is from $0.1 f_{ce}$ to $0.2 f_{ce}$ in the case

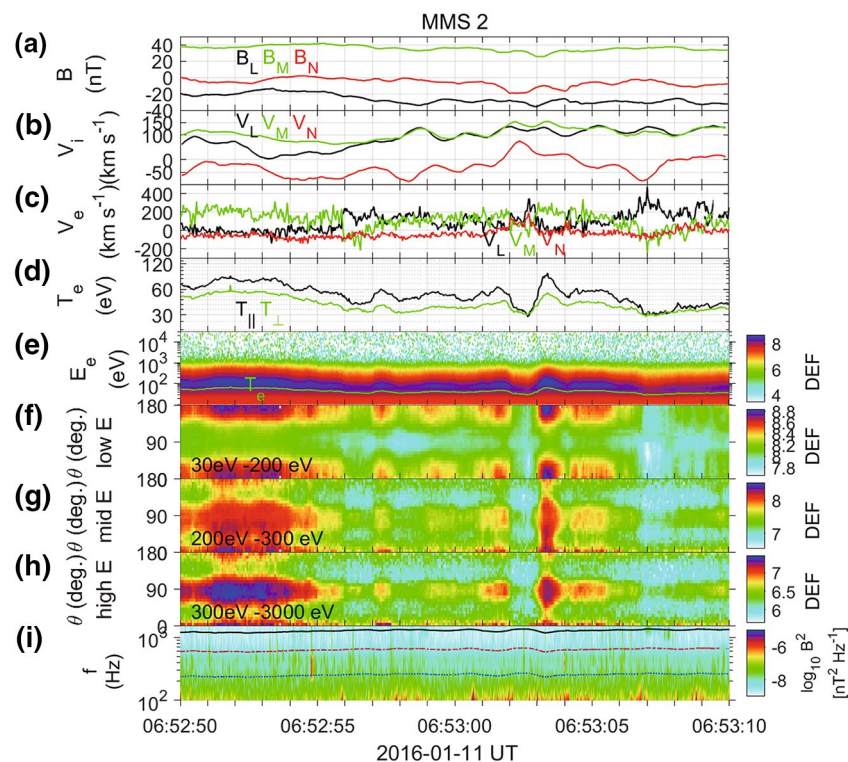


Figure 4. MMS2 measurements on reconnection central plane's magnetosheath side in LMN coordinates during 06:52:50–06:53:10 UT. Same format as Figure 3. LMN, Local Magnetic Normal; MMS, Magnetospheric Multiscale mission.

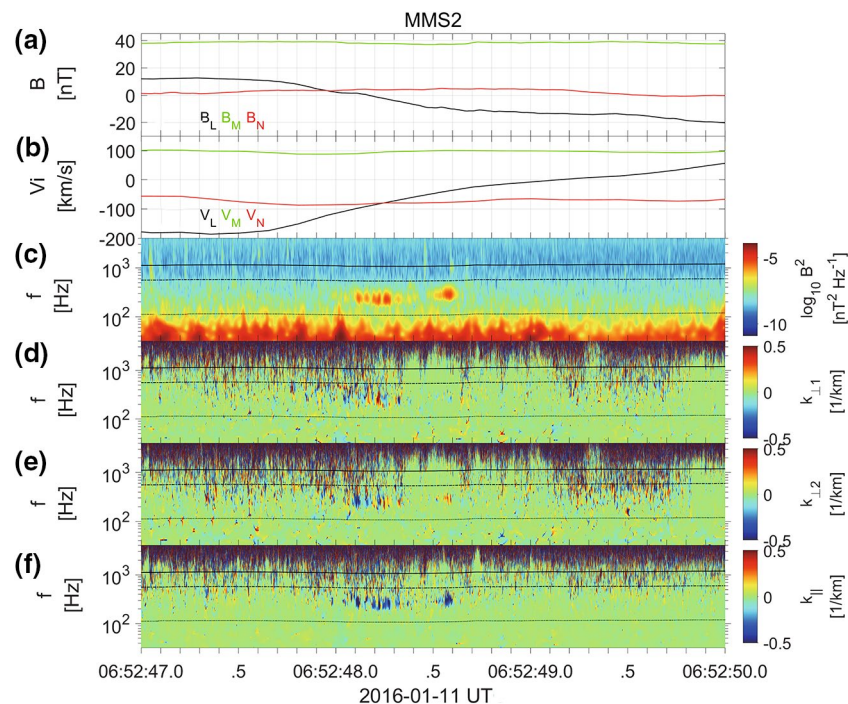


Figure 5. Wave analysis during 06:52:47–06:52:50 UT. (a and b) Magnetic field and ion bulk velocity in LMN coordinates; (c) the power spectral distribution of the magnetic field; (d-f) the spectrograms of wave vectors \mathbf{k} in the field-aligned coordinates. The horizontal lines in panel (c-f) represent the f_{ce} , 0.5 f_{ce} , and 0.1 f_{ce} , respectively.

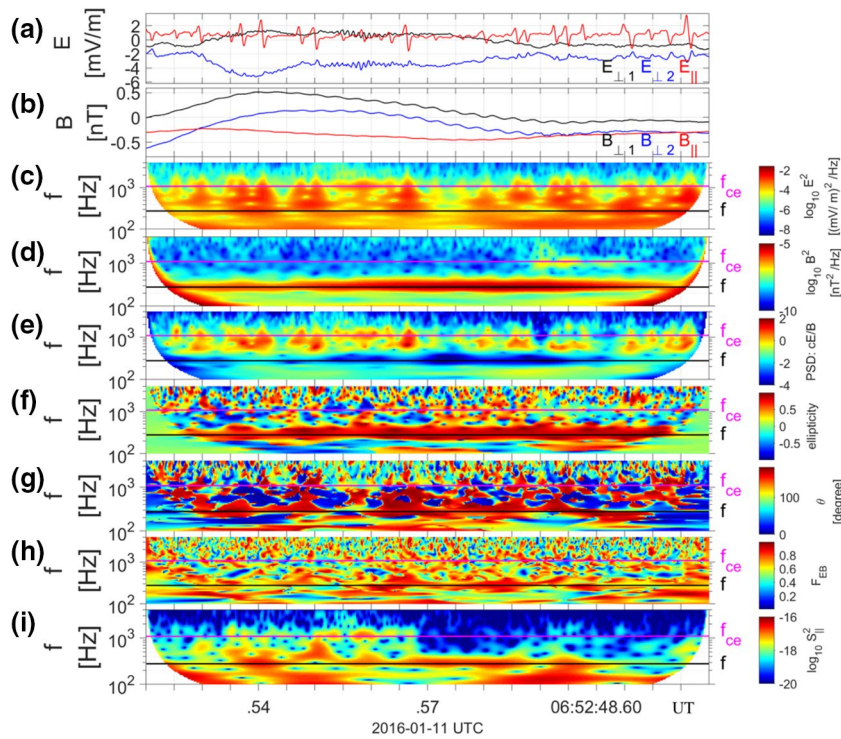


Figure 6. The power spectral distributions (PSD) and other properties of electromagnetic waves during 06:52:48.52–06:52:48.62 UT. (a) Electric field components; (b) perturbed magnetic field components; (c) PSD of electric field; (d) PSD of magnetic field; (e) the ratio of electric over magnetic wavefield; (f) ellipticity; (g) θ : wave propagation angle (between wave vectors and the background magnetic field); (h) electromagnetic planarity F_{EB} ; (i) field-aligned component of Poynting fluxes. In panel (c–i), the frequency f corresponding to the maximum of magnetic PSD and the f_{ce} are marked by black and pink horizontal lines, respectively.

of positive growth rate, which is reasonably agreed with the observations ($\sim 0.25 f_{ce}$ corresponding to the maximum of magnetic PSD).

4. Discussions and Conclusions

We present MMS observations of the beam-driven whistler mode waves in the magnetic reconnection region at the dayside magnetopause on January 11, 2016. Due to Hall magnetic field perturbations, the reconnection electric field contributes to the acceleration potential $\Phi_{||}$, resulting in the formation of counter-streaming electron beams in the reconnection inflow region (Egedal et al., 2011). The counter-streaming electron beams are mostly observed on the low-density magnetospheric side of the reconnection central plane, with a few exceptions, consistent with the simulation results (J. Huang et al., 2008).

The whistlers are observed in the presence of counter-streaming electron beams in the medium energy range (200–300 eV). We hypothesize that the whistlers are driven by the electron beams based on the following observational evidence. First, the speeds of electron parallel beams ($V_{\text{para}} \sim 6,600 \text{ km/s}$) and antiparallel beams ($V_{\text{anti}} \sim -6,900 \text{ km/s}$) are close to and slightly larger than the phase speeds of whistlers ($V_{\text{phase}} \sim -5,700 \text{ km/s}$), indicating the existence of Landau resonance and energy transfer between plasmas and waves. Second, the observed dispersion relations using the SVD method are in reasonable agreement with results derived in the linear homogenous kinetic plasma model by the BO method. Moreover, the kinetic growth rate is positive in the wave frequency range. Therefore, one possibility of wave generation is that the electron beams resonate with the waves contributing to the inverse Landau damping process (Li et al., 2016; Wilder et al., 2017). The electron parallel beams (in principle) can drive whistlers. However,

Table 1
The Electrons Parameters by Fitting the Bi-maxwellian Distributions

Electron populations	Density (cm^{-3})	T_{\parallel} (eV)	T_{\perp} (eV)	v_b (km/s)
Parallel beam	1.12	13	30	6,600
Antiparallel beam	1.09	10.5	24	-6,900
High-energy background electrons	10	85	60	0
Low-energy background electrons	2.5	7	5.5	0

the antiparallel beams are more important in this event, maybe due to higher flow speed and lower thermal velocity. In whistler generation processes, plasma energy is converted into wave energy.

In the high energy range (300–3,000 eV), the whistlers are observed simultaneously with electron pitch-angle scattering. Plasmas can be scattered and exchange energy with waves through cyclotron resonance and transit time damping interactions. For whistlers, electron cyclotron wave-particle interactions are most effective when the electron velocity parallel to the background magnetic field, $v_{\parallel,e}$, satisfies the cyclotron resonance condition,

$$k_{\parallel}v_{\parallel,e} = \omega_r - |\omega_{ce}| = 2\pi(f_r - |f_{ce}|),$$

where k_{\parallel} , ω_r (f_r) and ω_{ce} (f_{ce}) are the parallel wave vector, the wave frequency which is a function of k_{\parallel} , and the electron cyclotron frequency, respectively (Saito & Gary, 2007). For the sake of simplicity, we utilize the 95% confidence interval of observational parallel wave vectors $k_{\parallel} = (-0.43 \pm 0.014)/d_e$, the wave frequency $f_r \sim (100, 500)$ Hz, and $f_{ce} \sim 1100$ Hz to estimate $v_{\parallel,e}$, where the average electron skin depth $d_e \sim 1.4$ km. Thus, we can get $v_{\parallel,e} \sim (12000, 20000)$ km/s, corresponding to $T_e \sim (800, 2300)$ eV. Such an electron energy range is consistent with the observations. It can be seen that electron pitch-angle scattering occurs at higher energies than the wave excitation. The electron pitch-angle scattering by whistlers can isotropize electrons and exchange energy between plasmas and waves.

In summary, our research will add further quantitative understanding of the beam-driven whistler mode waves in the reconnection context. More detailed physical processes of beam-driven whistlers need further investigation in our future studies.

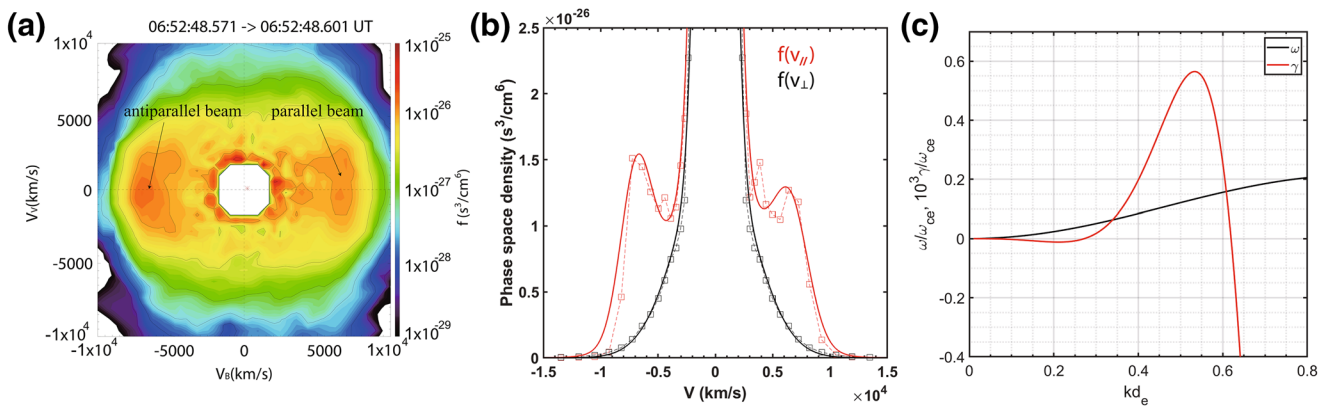


Figure 7. (a) two-dimensional $V_B - V_V$ cut of electron distribution during 06:52:48.571–06:52:48.601 UT, where V_B is parallel to the magnetic field and V_V is in the $(\mathbf{v} \times \mathbf{b}) \times \mathbf{b}$ direction (\mathbf{b} and \mathbf{v} are the unit vectors of the magnetic field and the electron bulk velocity). The whistlers are observed in this duration. The arrows point at the parallel and antiparallel beams, respectively. (b) The phase space density in the parallel (red) and perpendicular (black) directions. The dashed lines represent the observed distributions, and the solid lines represent the fitted distributions. (c) The dispersion relation (black) and growth rate γ (red) of whistlers from the BO method (Xie, 2019).

Data Availability Statement

MMS data and WIND data are found online (<https://spdf.gsfc.nasa.gov/>); The data analysis software named SPADAS are available at <http://themis.ssl.berkeley.edu>.

Acknowledgments

This work was supported by NSFC grants 11975038. We would like to thank the MMS spacecraft team, the WIND spacecraft team, the NASA's Coordinated Data Analysis Web (CDAWeb, <https://cdaweb.gsfc.nasa.gov/>) and the Chinese Meridian Project for their data access. We acknowledge the plasma astrophysics group led by Huirong Yan in Deutsches Elektronen Synchrotron (DESY).

References

- Burch, J. L., Moore, T. E., Torbert, R. B., & Giles, B. L. (2016). Magnetospheric multiscale overview and science objectives. *Space Science Reviews*, 199(1–4), 5–21. <https://doi.org/10.1007/s11214-015-0164-9>
- Cao, D., Fu, H. S., Cao, J. B., Wang, T. Y., Graham, D. B., Chen, Z. Z., et al. (2017). MMS observations of whistler waves in electron diffusion region. *Geophysical Research Letters*, 44(9), 3954–3962. <https://doi.org/10.1002/2017GL072703>
- Contel, O. Le, Roux, P. L. A., Alison, C. C. D., Meslier, L. M. L., Vassal, A. G. M. C., Needell, R. B. T. J., et al. (2016). The Search-Coil Magnetometer for MMS. *Space Science Reviews*, 257–282. <https://doi.org/10.1007/s11214-014-0096-9>
- Deng, X. H., & Matsumoto, H. (2001). Rapid magnetic reconnection in the earth's magnetosphere mediated by whistler waves. *Nature*, 410(6828), 557–560. <https://doi.org/10.1038/35069018>
- Drake, J. F., Shay, M. A., & Swisdak, M. (2008). The Hall fields and fast magnetic reconnection. *Physics of Plasmas*, 15(4), 042306. <https://doi.org/10.1063/1.2901194>
- Dungey, J. W. (1961). Interplanetary magnetic field and the auroral zones. *Physical Review Letters*, 6(2), 47–48. <https://doi.org/10.1103/PhysRevLett.6.47>
- Egedal, J., Le, A., Pritchett, P. L., & Daughton, W. (2011). Electron dynamics in two-dimensional asymmetric anti-parallel reconnection. *Physics of Plasmas*, 18(10), 102901. <https://doi.org/10.1063/1.3646316>
- Ergun, R. E., Tucker, S., Westfall, J., Goodrich, K. A., Malaspina, D. M., Summers, D., et al. (2016). The axial double probe and fields signal processing for the MMS Mission. *Space Science Reviews*, 199(1–4), 167–188. <https://doi.org/10.1007/s11214-014-0115-x>
- Fuselier, S. A., Trattner, K. J., & Petrinec, S. M. (2011). Antiparallel and component reconnection at the dayside magnetopause. *Journal of Geophysical Research*, 116(10), 1–14. <https://doi.org/10.1029/2011JA016888>
- Gary, S. P., Scime, E. E., Phillips, J. L., & Feldman, W. C. (1994). The whistler heat flux instability: Threshold conditions in the solar wind. *Journal of Geophysical Research*, 99(12), 23391–23399. <https://doi.org/10.1029/94JA02067>
- Goldman, M. V., Newman, D. L., Lapenta, G., Andersson, L., Gosling, J. T., Eriksson, S., et al. (2014). Čerenkov emission of quasiparallel whistlers by fast electron phase-space holes during magnetic reconnection. *Physical Review Letters*, 112(14), 1–5. <https://doi.org/10.1103/PhysRevLett.112.145002>
- Grinsted, A., Moore, J. C., & Jevrejeva, S. (2004). Application of the cross wavelet transform and wavelet coherence to geophysical time series. *Nonlinear Processes in Geophysics*, 11(5/6), 561–566. <https://doi.org/10.5194/npg-11-561-2004>
- Huang, J., Ma, Z. W., & Li, D. (2008). Debye-length scaled structure of perpendicular electric field in collisionless magnetic reconnection. *Geophysical Research Letters*, 35(10), 1–5. <https://doi.org/10.1029/2008GL033751>
- Huang, H., Yu, Y., Dai, L., & Wang, T. (2018). Kinetic alfvén waves excited in two-dimensional magnetic reconnection. *Journal of Geophysical Research: Space Physics*, 123(8), 6655–6669. <https://doi.org/10.1029/2017JA025071>
- Kennel, C. F., & Petschek, H. E. (1966). Limit on stably trapped particle fluxes. *Journal of Geophysical Research*, 71(1), 1–28. <https://doi.org/10.1029/JZ071i001p00001>
- Khotyaintsev, Y. V., Cully, C. M., Vaivads, A., André, M., & Owen, C. J. (2011). Plasma jet braking: Energy dissipation and non-adiabatic electrons. *Physical Review Letters*, 106(16), 1–4. <https://doi.org/10.1103/PhysRevLett.106.165001>
- Lepping, R. P., Acuña, M. H., Burlaga, L. F., Farrell, W. M., Slavin, J. A., Schatten, K. H., et al. (1995). The WIND magnetic field investigation. *Space Science Reviews*, 71(1–4), 207–229. <https://doi.org/10.1007/BF00751330>
- Li, W., Mourenas, D., Artemyev, A. V., Bortnik, J., Thorne, R. M., Kletzing, C. A., et al. (2016). Unraveling the excitation mechanisms of highly oblique lower band chorus waves. *Geophysical Research Letters*, 43(17), 8867–8875. <https://doi.org/10.1002/2016GL070386>
- Lin, R. P., Anderson, K. A., Ashford, S., Carlson, C., Curtis, D., Ergun, R., et al. (1995). A three-dimensional plasma and energetic particle investigation for the wind spacecraft. *Space Science Reviews*, 71(1–4), 125–153. <https://doi.org/10.1007/BF00751328>
- Lindqvist, P. A., Olsson, G., Torbert, R. B., King, B., Granoff, M., Rau, D., et al. (2016). The spin-plane double probe electric field instrument for MMS. *Space Science Reviews*, 199(1–4), 137–165. <https://doi.org/10.1007/s11214-014-0116-9>
- Pollock, C., Moore, T., Jacques, A., Burch, J., Gliese, U., Saito, Y., et al. (2016). Fast Plasma Investigation for magnetospheric multiscale. *Space Science Reviews*, 199(1–4), 331–406. <https://doi.org/10.1007/s11214-016-0245-4>
- Russell, C. T., Anderson, B. J., Baumjohann, W., Bromund, K. R., Dearborn, D., Fischer, D., et al. (2016). The Magnetospheric multiscale magnetometers. *Space Science Reviews*, 199(1–4), 189–256. <https://doi.org/10.1007/s11214-014-0057-3>
- Saito, S., & Gary, S. P. (2007). Whistler scattering of suprathermal electrons in the solar wind: Particle-in-cell simulations. *Journal of Geophysical Research*, 112(6), 1–12. <https://doi.org/10.1029/2006JA012216>
- Santolík, O., Parrot, M., & Lefèuvre, F. (2003). Singular value decomposition methods for wave propagation analysis. *Radio Science*, 38(1), 1010. <https://doi.org/10.1029/2000RS002523>
- Sonnerup, B. U. Ö., Papamastorakis, I., Paschmann, G., & Lühr, H. (1987). Magnetopause properties from AMPTE/IRM observations of the convection electric field: Method development. *Journal of Geophysical Research*, 92(A11), 12137. <https://doi.org/10.1029/ja092ia11p12137>
- Sonnerup, B., & Scheible, M. (1998). Minimum and maximum variance analysis. Analysis Methods for Multi-Spacecraft Data. Retrieved from <http://ankaa.unibe.ch/forads/sr-001-08.pdf>. <http://ankaa.unibe.ch/forads/sr-001-08.pdf>
- Vörös, Z., Yordanova, E., Graham, D. B., Khotyaintsev, Y. V., & Narita, Y. (2019). MMS Observations of whistler and lower hybrid drift waves associated with magnetic reconnection in the turbulent magnetosheath. *Journal of Geophysical Research: Space Physics*, 124(11), 8551–8563. <https://doi.org/10.1029/2019JA027028>
- Wang, X., Bhattacharjee, A., & Ma, Z. W. (2000). Collisionless reconnection: Effects of Hall current and electron pressure gradient. *Journal of Geophysical Research*, 105(A12), 27633–27648. <https://doi.org/10.1029/1999JA000357>
- Wilder, F. D., Ergun, R. E., Newman, D. L., Goodrich, K. A., Trattner, K. J., Goldman, M. V., et al. (2017). The non-linear behavior of whistler waves at the reconnecting dayside magnetopause as observed by the Magnetospheric Multiscale mission: A case study. *Journal of Geophysical Research: Space Physics*, 122(5), 5487–5501. <https://doi.org/10.1002/2017JA024062>

- Xiao, C. J., Wang, X. G., Pu, Z. Y., Ma, Z. W., Zhao, H., Zhou, G. P., et al. (2007). Satellite observations of separator-line geometry of three-dimensional magnetic reconnection. *Nature Physics*, 3(9), 609–613. <https://doi.org/10.1038/nphys650>
- Xie, H. S. (2019). BO: A unified tool for plasma waves and instabilities analysis. *Computer Physics Communications*, 244, 343–371. <https://doi.org/10.1016/j.cpc.2019.06.014>
- Zhou, M., Ashour-Abdalla, M., Berchem, J., Walker, R. J., Liang, H., El-Alaoui, M., et al. (2016). Observation of high-frequency electrostatic waves in the vicinity of the reconnection ion diffusion region by the spacecraft of the Magnetospheric Multiscale (MMS) mission. *Geophysical Research Letters*, 43(10), 4808–4815. <https://doi.org/10.1002/2016GL069010>